

Oscillatory quasistatic shear deformation of amorphous materials: a mesoscopic approach

Chen Liu,¹ Ezequiel E. Ferrero,² Eduardo A. Jagla,³ Kirsten Martens,⁴ Alberto Rosso,⁵ and Laurent Talon⁶

¹*Laboratoire de Physique de l'Ecole Normale Supérieure, Paris, France*

²*Instituto de Nanociencia y Nanotecnología, CNEA-CONICET,*

Centro Atómico Bariloche, (R8402AGP) San Carlos de Bariloche, Río Negro, Argentina.

³*Centro Atómico Bariloche, Instituto Balseiro, Comisión Nacional de Energía Atómica, CNEA, CONICET, UNCUYO, Av. E. Bustillo 9500 R8402AGP S. C. de Bariloche, Río Negro, Argentina*

⁴*Univ. Grenoble Alpes, CNRS, LIPhy, 38000 Grenoble, France*

⁵*LPTMS, CNRS, Univ. Paris-Sud, Université Paris-Saclay, 91405 Orsay, France*

⁶*FAST, CNRS, Univ. Paris-Sud, Université Paris-Saclay, 91405 Orsay, France*

(Dated: September 11, 2022)

Recent atomistic simulations have identified novel rheological properties on amorphous materials under quasi-static oscillatory shear. Using a coarse-grained model based on the evolution of a continuum strain field, we characterize these properties in the stationary limit, reached after several oscillations. We built a ‘phase diagram’ depending on two control parameters: the strain amplitude γ_{\max} and the degree of annealing E_{init} . At small amplitudes, poorly annealed materials display *shear annealing* behavior, appearing better and better annealed as γ_{\max} is increased. Ultra-stable materials are instead insensitive to those oscillations. Above a critical strain amplitude γ_c , that increases with annealing level, the melting of the material in a localized band of finite width is observed. Inside the band, the material flows, outside the band there is a marginal solid independent of the initial degree of annealing. Such a ‘phase transition’ at γ_c between a solid and a mixed phase is discontinuous. The transient dynamics before reaching the steady state is also studied.

INTRODUCTION

Amorphous solids are a vast class of materials, common in nature and ubiquitous for human applications. Their physical behaviour can be rationalized in terms of the annealing protocol: poorly annealed systems, such as emulsions, foams or gels, are soft and ductile, while well annealed materials such as metallic glasses, ceramics and silica are hard and brittle [1, 2]. When a large deformation is applied [3, 4] soft materials tend to melt homogeneously into a liquid, while hard materials fail at a material dependent strain, γ_f . Above γ_f -if fracture is prevented- a liquid shear band spreads leaving the rest of the system in its original solid phase. Whether these two regimes are separated by a genuine critical point (namely a critical degree of annealing) [3] or rather a crossover among a continuum of yielding transitions (highly dependent on finite-size effects) [5] is a matter of current discussion (see also [4]).

Here we study instead the case of oscillatory quasistatic shear and show that, in the steady state, the phase diagram and the presence of a sharp transition is much less ambiguous compared to the case of a uniform large shear. The oscillatory protocol was originally motivated by the possibility to encode information in amorphous solids after a specific training [6], but it also showed the presence of a yielding transition [7–9] as a function of the strain amplitude γ_{\max} . Two behaviours, peculiar of this protocol, have been identified: First, for moderate strain amplitude γ_{\max} the material appears better and better annealed [10, 11] as the number of cycles n increases, a fact that can be even exploited to obtain a desired mechanical response subsequently [12]. Second, the ex-

istence of a critical amplitude, γ_c , above which further shear annealing is prevented and a shear band appears [3, 10]. Most of the dedicated works are molecular dynamics simulations of collection of polydisperse repulsive particles and focus on the trajectories of the particles in the stationary limit of large n : for small γ_{\max} all particles have perfect periodic trajectories that have been mathematically characterized [13], while, above γ_c , a fraction of particles display a chaotic behavior [14], associated to the presence of the shear band instability [3, 10]. Inside the shear band, the material is liquid and particles have a finite diffusion coefficient (with respect to the number of cycles n) while in the solid phase the diffusion coefficient is zero and particles remain localized in periodic trajectories [9]. However despite rapidly growing numerical evidence and theoretical proposals [3, 10, 11, 13–24], the nature of the emerging ‘phases’, the transition among them and the role of the initial degree of annealing call for understanding. It is also important to establish a clear connection between the response to oscillatory shear and the one observed under uniform strain. To achieve this one needs of approaches beyond the molecular dynamics simulations that have dominated the scene so far.

In this work, we study the oscillatory shear protocol using a mesoscopic model based on the evolution of a scalar strain field in a disordered potential. These potentials account both for the local elastic behavior and for the presence of plastic instabilities. Initial sample preparation at different levels of annealing is reproduced by tuning the disorder energy (low energies correspond to better annealed systems). Within this picture, the strain field behaves as a manifold propagating in a disordered medium [25–27]. However, at variance with elastic

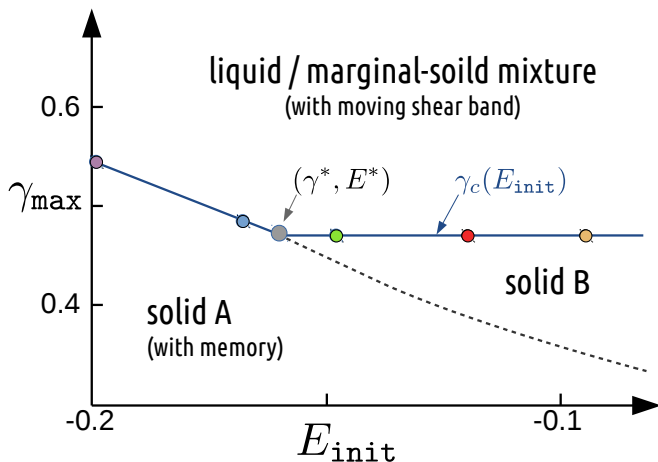


Figure 1. Phase diagram of amorphous materials under oscillatory shear in the stationary limit. The control parameters are the amplitude of the oscillations γ_{\max} and the initial degree of annealing, E_{init} . Three phases are identified: the solid A has physical properties strongly reminiscent of the initial state of the material. The solid B is completely independent of the initial annealing and evolves continuously up to γ^* where it becomes a marginal solid. Above γ_c , the solid becomes unstable and an erratic finite shear band coexists with the marginal solid phase. We determined γ_c for different degrees of annealing, indicated in the diagram by colored circles ($E_{\text{init}} \approx -0.095$ (chocolate), -0.12 (red), -0.149 (chamelon), -0.168 (blue), -0.199 (plum)).

interfaces studied in the context of the depinning transition [28–30] two important ingredients should be considered: First, the non-monotonic behavior of the elastic interactions; here fulfilled by using an Eshelby propagator. Secondly, the nature of the disorder, not induced by quenched impurities but originated instead from the random positions of the particles of the material. In our implementation then, the local disorder changes irreversibly, even if the strain manifold revisits the same location.

Our model allows to unveil the ‘phase diagram’ reached in the stationary limit of the oscillatory deformation and summarised in Fig.1. The diagram separates different steady ‘phases’ according to two basic characteristics of the deformation protocol: the initial annealing level E_{init} and the deformation amplitude γ_{\max} . First, a transition line, $\gamma_c(E_{\text{init}})$, separates a solid phase at small amplitudes from a solid-liquid mixture (composed by a fluid shear band immersed in a solid) at larger amplitudes. We identify a critical degree of annealing $E_{\text{init}} = E^*$ such that: When $E_{\text{init}} > E^*$ the solid is shear annealed by increasing γ_{\max} , up to an amplitude $\gamma_c(E_{\text{init}}) = \gamma^*$ at which it reaches its minimal energy that coincides with E^* . We call this state *marginal solid* as, for larger γ_{\max} , a shear band instability sets in, giving place to the solid-liquid mixed phase. On the other hand, when $E_{\text{init}} < E^*$, no shear annealing is observed and the critical strain amplitude $\gamma_c(E_{\text{init}})$, greater than γ^* , increases with the degree

of annealing (i.e., increases as E_{init} decreases). If we compare with the uniform strain case, the homogeneous melting at large deformations is never observed with periodic shear. Yet, the liquid state inside the shear band is identical in the two protocols. Moreover, periodic shear simulations show the existence of two novel type of solids when $E_{\text{init}} > E^*$: at small γ_{\max} the sheared solid conserves memory of its initial degree of annealing (solid A), while at larger γ_{\max} this memory is completely lost (solid B). In the following, we present and discuss the results of our simulations. Results correspond to systems of size 128×128 unless otherwise specified.

RESULTS

Uniform shear

We first recall the results known in the case of a monotonically increased shear deformation. We will see that some of the quantities defined with this protocol play also an important role in presence of oscillations.

In Fig.2(a), we show stress-strain curves for individual samples prepared at different degrees of annealing. After an initial linear elastic response of slope ≈ 0.91 (value explained in Methods), all samples reach a common plateau corresponding to the yield stress $\Sigma_y \approx 0.375(\pm 0.003)$. The characteristic strain where plasticity becomes important can be estimated using the value of the initial slope as $\gamma = \gamma_y = \Sigma_y/0.91 \simeq 0.413$. Poorly annealed materials display a monotonic ‘transition’ from an elastic solid to a liquid close to γ_y . Well annealed systems, on the other hand, remain elastic above γ_y up to a failure strain γ_f where a non-monotonic sharp overshoot occurs. The value of γ_f and the subsequent stress jump are larger as the initial condition is better and better annealed.

It is useful to decompose the total energy of the material in two contributions:

$$E_{\text{tot}}(E_{\text{init}}, \gamma) = E_{\text{sf}} + \Sigma^2/(4\mu), \quad (1)$$

where the second term is the elastic energy of the deformation with μ the shear modulus (here $\mu = 1/2$), and E_{sf} is the energy of the material at mechanical equilibrium when the stress is zero (we call it ‘stress-free energy’ E_{sf}). When looking to the system’s stress-free energy (see Fig.2(b)), we observe that poorly annealed samples (those which do not display a failure) reach a common energy plateau $E_{\text{liq}} \approx -0.122(\pm 0.001)$, while well annealed samples display different and slowly-evolving transient regimes. These differences can be understood as follows: poorly annealed systems melt at deformations around γ_y into a non-Newtonian liquid which has no memory of the initial degree of annealing (see Fig.2 bottom-left). In well annealed systems, instead, the non-Newtonian liquid is localised within a shear band and the solid part is unchanged, insensitive to the deformation (see Fig.2 bottom-right). When γ is increased further, the band

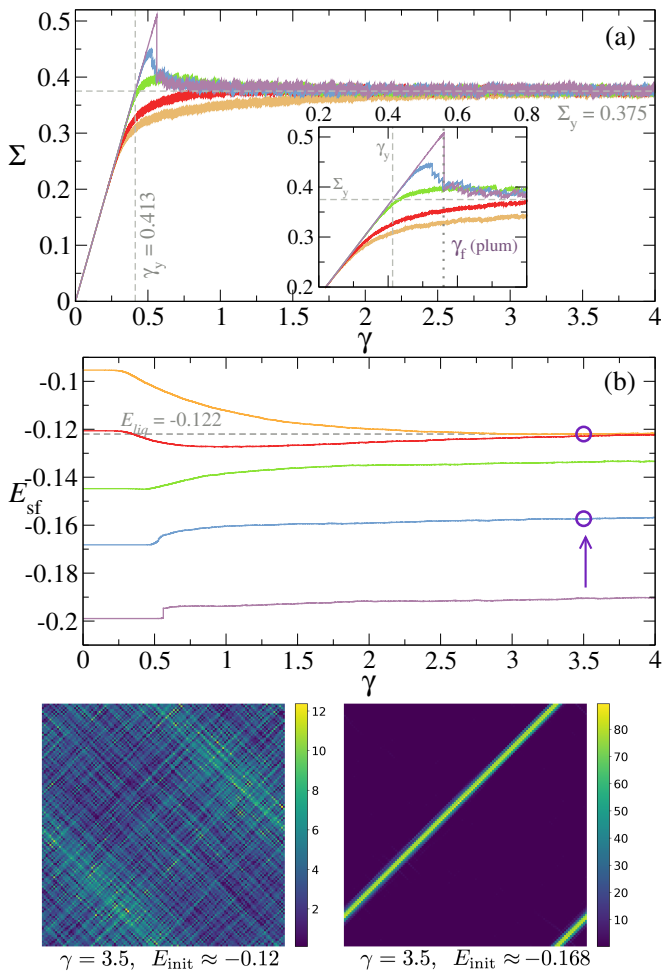


Figure 2. Uniform shear deformation for different degrees of initial annealing ($E_{init} \approx -0.095$ (chocolate), -0.12 (red), -0.149 (chamelon), -0.168 (blue), -0.199 (plum)). (a) Stress-strain curves for different initial degrees of annealing. The yield stress $\Sigma_y = 0.375$ defined as the plateau is also indicated. (b) Evolution of the stress-free energy $E_{sf} = E(\Sigma) - \Sigma^2/(4\mu)$ during the deformation. The stationary plateau $E_{liq} = -0.122$ is also indicated. **Bottom:** Colormap of the local deformation field at $\gamma = 3.5$ for two degree of annealing, circles in (b).

widens. As discussed in [31], we expect $w(\gamma) \propto \sqrt{\gamma - \gamma_f}$. Eventually, for very large γ , the band width reaches the system size and the whole sample lose memory of the initial condition converging to the stationary value E_{liq} .

Oscillatory shear

We now investigate the oscillatory protocol where the material is deformed quasi-statically with a strain increasing up to γ_{max} and then reversed up to $-\gamma_{max}$. The protocol is repeated periodically until a stationary state is reached. In the following we explore what we call with some caution the ‘phase diagram’ of the stationary

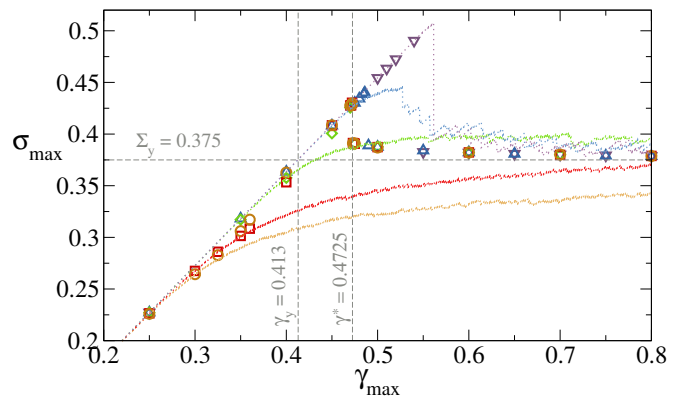


Figure 3. Stress value, σ_{max} , at γ_{max} in the oscillatory steady state as a function of the strain amplitude γ_{max} . Different colors and symbols code for systems of different degrees of annealing ($E_{init} \approx -0.095$ (chocolate circles), -0.12 (red squares), -0.149 (chamelon diamonds), -0.168 (blue up-triangles), -0.199 (plum down-triangles)). For comparison, the uniform strain curves of Fig.2 are included as light color lines for each initial condition.

state by varying γ_{max} and E_{init} . Compared to uniform shear, we see that with oscillatory shear we recover a mixed phase with a shear band made of the same non-Newtonian liquid (and thus the same γ_y , Σ_y , E_{liq}); but the solid phase(s), the location of the transition lines and the physics of the shear bands are strongly modified.

Stationary properties

In Fig. 3, we show the steady-state stress σ_{max} vs. γ_{max} . at variance with the uniform shear case, even poorly annealed samples, show a sharp jump of the steady stress value at a critical strain amplitude $\gamma_c(E_{init})$. Interestingly, the moderately annealed samples ($E_{init} = -0.095$, -0.12 and -0.149) fail at the same $\gamma_c = \gamma^* = 0.4725$, independently on the initial degree of annealing, while the more stable samples ($E_{init} = -0.168$ and -0.199) display a later and stronger failure at $\gamma_c(E_{init}) \approx \gamma_f(E_{init}) > \gamma^*$. In both cases, beyond the failure, the system develops a permanent liquid shear band embedded in a solid phase.

Figure 4 displays the stationary value of the stress-free energy E_{sf} as a function of γ_{max} . For small values of γ_{max} , the material remains solid and E_{sf} strongly depends on the initial degree of annealing. We call this phase ‘solid A’. Increasing γ_{max} , but still in the solid phase ($\gamma_{max} < \gamma_c$), two scenarios, separated by a critical initial annealing $E^* = -0.16$, are observed:

- For $E_{init} > E^*$, the energy E_{sf} of different samples collapse to a common curve (blue dashed line). The solid phase, that we called ‘solid B’, is independent on the initial degree of annealing and has a shear annealing behavior up to γ^* . There the solid phase become marginal as the energy reaches the minimal

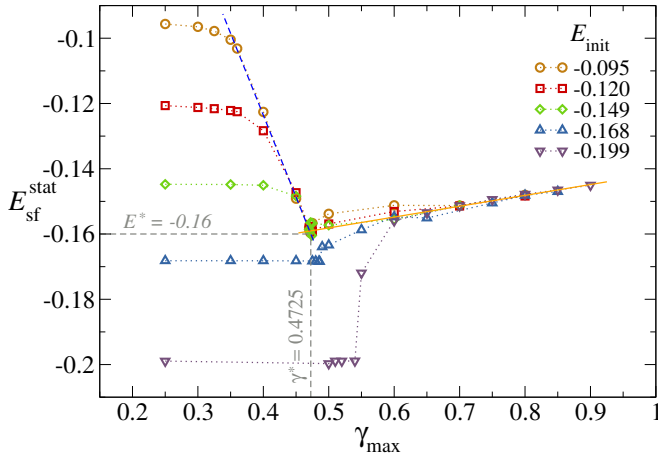


Figure 4. Stress-free energy as a function of strain in the oscillatory steady state, for different annealing levels E_{init} as indicated by the labels. Yellow solid line corresponds to Eq.3. Purple dashed line indicates the stress-free energy of solid B.

value E^* , which corresponds to the maximal shear annealing.

- For $E_{\text{init}} < E^*$, E_{sf} doesn't evolve with γ_{max} in the whole solid phase. No shear annealing is thus observed.

For $\gamma_{\text{max}} > \gamma_c$, a shear band occurs in both cases. In Fig. 5 we study the total energy E as a function of γ during a steady oscillation between $\pm\gamma_{\text{max}}$. While in the solid phase ($\gamma_{\text{max}} < \gamma_c$), the energy displays a single parabolic shape, corresponding to an elastic behavior, in the mixed phase ($\gamma_{\text{max}} > \gamma_c$), the energy has a butterfly shape: two shifted parabola are followed by a noisy plateau which reveals the presence of the Non-Newtonian liquid. The two parabolas have an extension of γ_y at both sides and the maximal stress, at $\pm\gamma_{\text{max}}$, saturates to Σ_y . This suggests that the shear band is made of a soft solid that melts at γ_y , when the stress reaches the value Σ_y . To confirm this picture, in Fig. 6 we show the stress free energy profile of the material across a section that is perpendicular to the shear band. The bell-shape corresponds to the shear band and reaches the liquid energy $E_{\text{liq}} = -0.122$ for all values of $\gamma_{\text{max}} > \gamma_c$. The width, w_s , increases with γ_{max} as already observed for the uniform shear protocol [31]. By analogy, we propose the fitting form:

$$w_s(\gamma_{\text{max}}) = a(\gamma_{\text{max}} - \gamma_0)^\alpha. \quad (2)$$

As for uniform shear, the good collapse (inset of Fig. 6) is found for $\alpha = 1/2$, so the width is independent of the system size and fraction of the liquid in the mixture is sub-extensive. The mixed phase is however different from the failure observed with uniform protocols (where $\gamma_0 = \gamma_f$) for two important aspects. First, from the fit, γ_0 identifies with γ_y instead of γ^* . This implies that, at the transition, the shear band has a finite width as

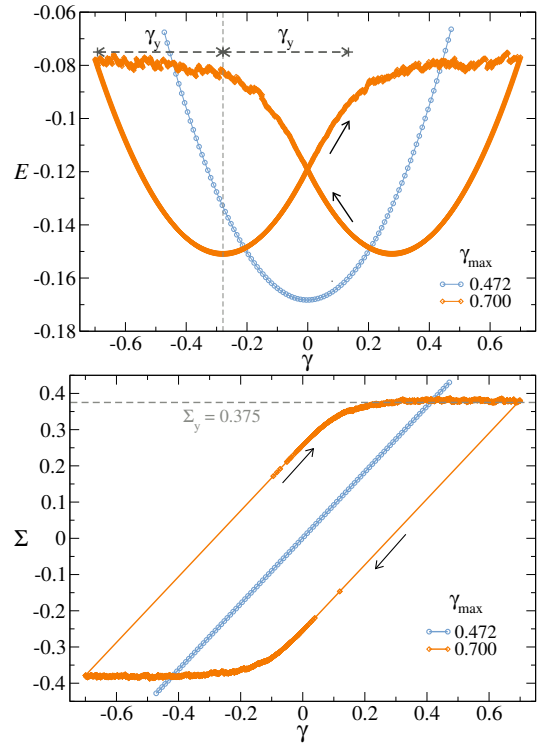


Figure 5. **Top:** Energy versus strain in the oscillatory steady state (only one loop shown) for $\gamma_{\text{max}} = 0.45$ (light-blue circles) and $\gamma_{\text{max}} = 0.7$ (orange diamonds). The little black arrows mark the sense of the loop. **Bottom:** Stress as a function of strain in the oscillatory steady state for the same two amplitudes as above.

$\gamma_y < \gamma^*$, while in uniform shear protocol the band width vanishes at γ_f . Second, the energy profile is independent on the initial degree of annealing and the energy at the bottom of the bell-shape always coincides with the marginal solid energy E^* (only when $\gamma_{\text{max}} = 0.65$ the energy is slightly smaller because the stationary state is not yet reached). This allows to conclude that the mixture phase is completely independent on the initial degree of annealing: the stationary regime is composed of a large fraction of marginal solid at energy E^* and a shear band with the non-Newtonian liquid at energy E_{liq} . As E_{liq} is higher than E^* we can explain the monotonic growth of E_{sf} in terms of the growth of the shear band width with γ_{max} :

$$\begin{aligned} E_{\text{sf}} &\sim E^* \left(1 - \frac{w_s(\gamma_{\text{max}})}{L}\right) + E_{\text{liq}} \frac{w_s(\gamma_{\text{max}})}{L}, \\ &\sim E^* + (E_{\text{liq}} - E^*) \frac{a(\gamma_{\text{max}} - \gamma_y)^\alpha}{L}. \end{aligned} \quad (3)$$

Eq.3 has been tested in Fig. 4 (the yellow solid line).

Transient properties

Now we discuss the transient oscillatory dynamics. The stress-free energy E_{sf} as function of the number of

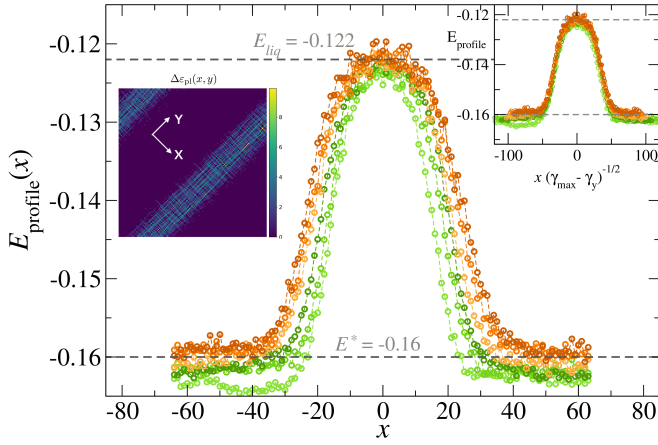


Figure 6. Averaged energy profile along the y -axis for different γ_{\max} . From light chamelon to dark orange: $\gamma_{\max} = 0.65, 0.7, 0.75, 0.8, 0.85, 0.9$. The origin of the x -axis has been adjusted with the maximum location. *Left inset*: plastic strain during a half cycle from $-\gamma_{\max}$ to γ_{\max} . One can distinguish a shear band embedded in a solid. *Right inset*: shear band collapse using Eq. 2 with $\gamma_0 = \gamma_y = 0.413$ and $\alpha = 1/2$.

oscillation cycles n for different initial states and amplitudes is shown in Fig.7. Below γ_c (**top panel**) When the oscillation amplitude is very small ($\gamma_{\max} = 0.25$) the material remains at its initial energy basin and no plastic events are observed. At a slightly larger amplitude ($\gamma_{\max} = 0.4$) the softest solids ($E_{\text{init}} = -0.095$ and -0.120) are shear annealed during the oscillations while the more annealed remain on their initial energy basin. When the amplitude approaches γ^* ($\gamma_{\max} = 0.47$), also the solid prepared at $E_{\text{init}} = -0.149$ shear-anneals. Therefore, our three softest samples are shear annealed reaching the solid B phase, while the two ultra-stable materials are unperturbed by the oscillation. The situation is different above γ_c (**middle panel**), where the stationary state is unique for any degree of annealing and the predicted value are well reached when $n \rightarrow \infty$.

The duration of the transient regime strongly depends on the annealing protocol and the critical annealing E^* , plays again an important role. Results for n_T , the number of cycles needed to reach the stationary state (defined by the condition $E_{\text{sf}}(n_T + 1) = E_{\text{sf}}(n_T)$) are shown in Fig. 7 (**bottom panel**), coming from the solid phase ($\gamma_{\max} < \gamma_c$):

- For poorly annealed samples ($E_{\text{init}} > E^*$), n_T diverges approaching γ^* , signaling a “dynamic slowing down”, typical of critical points. Nevertheless, at variance with standard phase transitions, the divergence is not a power-law, but is reasonably described by $n_T \propto \log[1/(\gamma_y^* - \gamma_y)]$.
- For well annealed samples ($E_{\text{init}} < E^*$), the stationary solid state is quickly reached as the initial energy basin is very deep. Only very close γ_c we observe a slight increase of n_T .

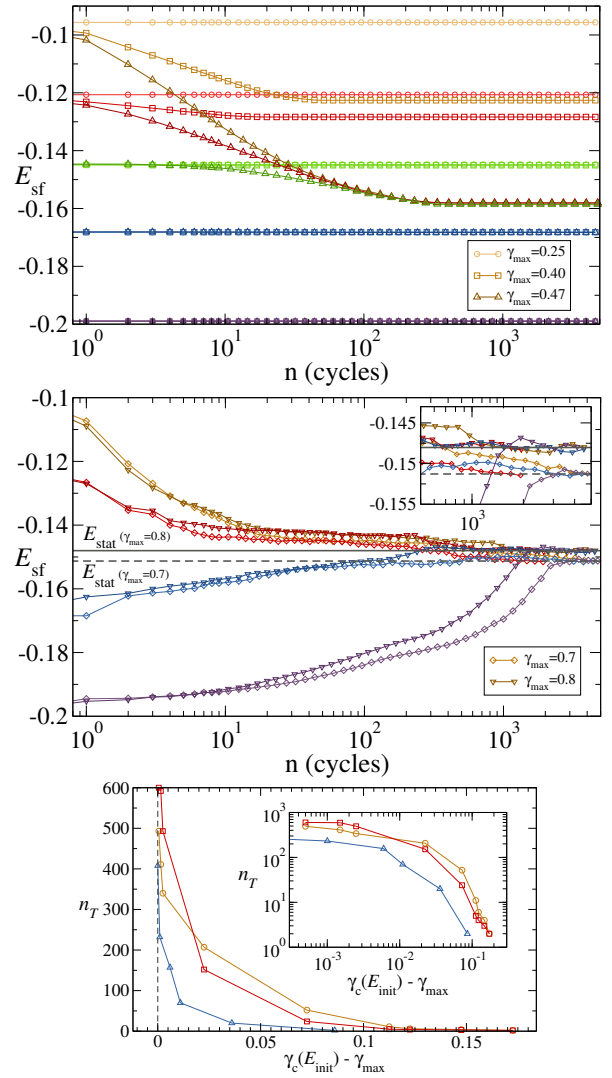


Figure 7. *Transient dynamics* Evolution of stress-free energy as a function of the number of cycles for different amplitudes. Colors indicate the annealing level ($E_{\text{init}} \approx -0.095$ (chocolate), -0.12 (red), -0.149 (chamelon), -0.168 (blue), -0.199 (plum)). **Top**: Solid phase with $\gamma_{\max} < \gamma^*$. At small amplitudes the system is trapped in its initial energy level, but as amplitude increases the system is able to seek for new stationary states corresponding to the solid in the phase B. **Middle**: Mixed phase ($\gamma_{\max} > \gamma^*$). The stationary state energy E_{stat} for the two values of γ_{\max} are also indicated. Their dependence on γ_{\max} is appreciable in the inset. **Bottom**: The number of cycles needed to reach to the steady solid state as a function of the distance of the solid-mixture transition, at γ_c . Inset is the log-log scale exhibition.

We now turn on the transient regime and the shear band dynamics for the mixed phase. In our simulations γ_{\max} is increased adiabatically and the transition is crossed when the sample is in the steady state at γ_c . In poorly annealed samples the onset of the shear band occurs when the solid is already marginal. As a consequence, the transient dynamics is very short: a shear

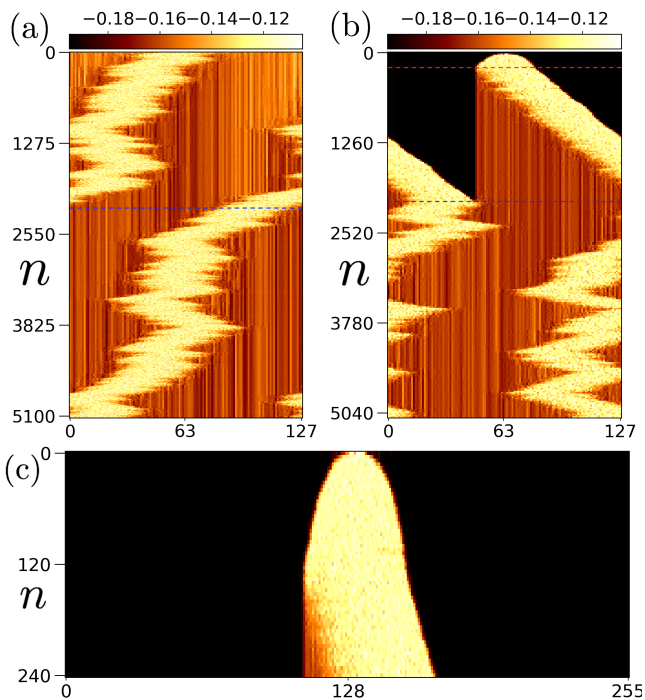


Figure 8. The energy profile across a section perpendicular to the shear band evolving as function of the number n of oscillation cycles. The light color region represents the position of the shear band with a higher energy. The amplitude of the oscillation is $\gamma_{\max} = 0.7$. Two samples are presented: (a) A poorly annealed sample with $E_{\text{init}} \approx -0.12$ and (b) well annealed sample with $E_{\text{init}} \approx -0.199$. The red dashed line in (b) indicate the complete creation of the band at $n \approx 220$. The blue dashed line indicates the moment when the band has visited the entire system for the first time at $n \approx 2200$ in (a) and at $n \approx 2100$ in (b). The early band growth regime for a well annealed sample of linear size $L = 256$.

band emerges rapidly during the early cycles reaching the stationary width $w_s(\gamma_{\max})$. Then it diffuses in the material (see the evolution of the energy profile Fig. 8a), with a mobility that increases with γ_{\max} . In well annealed systems ($E_{\text{init}} > E^*$) instead the transient is richer and we identify three dynamical regimes (see the evolution of the energy profile Fig. 8b):

- *Shear band emergence and growth.* The initial band growth is observed at the top of Fig. 8b and illustrated in more detail for a larger system ($L = 256$) in Fig. 8c. This initial coarsening of the shear band is studied in Fig.9 at different strain amplitudes. In all cases, the band width grows as $\sim n^{1/3}$ up to the plateau $\sim (\gamma_{\max} - \gamma_y)^{1/2}$ is reached.
- *Melting of a very annealed solid.* The now fully-formed shear band displays an initial ballistic motion preferentially invading the deeply annealed solid at a measurable average velocity and leaving behind the marginal solid.
- *Shear band diffusion.* When the shear band has

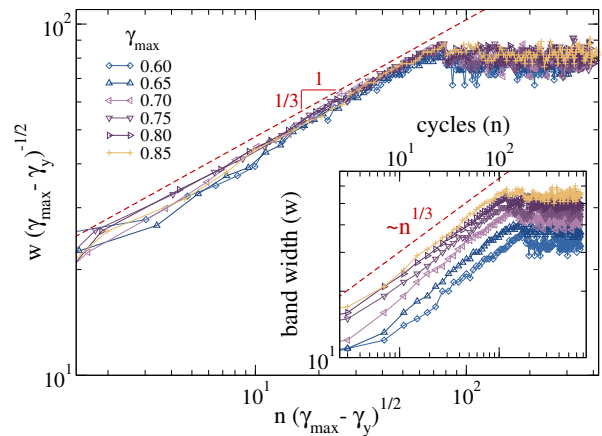


Figure 9. Shear-band width w as a function of the number of cycles n for different oscillation amplitudes $\gamma_{\max} = 0.60, 0.65, 0.70, 0.75, 0.80, 0.85$ as indicated in the labels. The initial condition is a well annealed solid ($E_{\text{init}} = -0.168$). Raw-data is shown in the inset, while the main panel shows the scaling $w(\gamma_{\max} - \gamma_y)^{-1/2}$ vs. $n(\gamma_{\max} - \gamma_y)^{1/2}$. The red dashed line of a power law $n^{1/3}$ for guiding eyes. These curves correspond to a system of size 256×256 .

visited the entire system, all the regions outside the band have been modified into the marginal solid component. The stationary state is reached and the band diffuses forever, maintaining its characteristic γ_{\max} -dependent width.

DISCUSSIONS

The mesoscopic model studied here allows to recover the phenomenology of the quasi static oscillatory protocol proposed by molecular dynamics simulations and go beyond. Indeed, with this method, the final stationary state can be characterized and compared with what obtained after a single uniform deformation.

The first big difference between the two protocols concerns ductile materials: while they melt homogeneously under uniform deformation, they undergo a sharp failure under quasi-static oscillations. This constitutes a discontinuous first-order-like transition (see also a similar observation in oscillatory sheared colloidal glasses [32]). However, the initial degree of annealing continues to play a fundamental role also in the case of oscillatory shear. In particular, a critical annealing E^* separates two qualitatively different behaviors:

Poorly annealed samples (those with $E_{\text{init}} > E^*$) become harder and harder when increasing γ_{\max} , reaching a solid phase (called solid B) independent on the initial annealing and with no counterpart in the uniform protocol. Then, at an annealing independent strain value γ^* , solid B becomes marginal: further shear annealing is prevented, a finite, but sub-extensive, shear band appears and permanently diffuses. While the liquid phase

inside the shear band is identical to the one observed in the uniform shear protocol, the marginal solid phase is much harder. The transition at γ^* displays critical features with a logarithmic divergent transient time. The emerging picture is consistent with the results of a simplified mesoscopic model very recently presented by S. Sastry [33]. However, in such approximation the elastic interaction between the different degrees of freedom are fully neglected, which prevents the formation of a shear band and thus the description of the mixed phase.

Well annealed samples (with $E_{\text{init}} < E^*$) are instead quite insensitive to oscillations up to the annealing-dependent critical amplitude $\gamma_c(E_{\text{init}}) > \gamma^*$. There, a large failure occurs as already observed in [3, 10]. Our numerical method allows to characterize the dynamics of the shear band in the mixed phase. We identified three distinct regimes: (i) the shear band formation with a width that grows as $n^{1/3}$, (ii) the melting of the well annealed solid invaded ballistically by the fully-formed shear band, and (iii) the stationary state with a diffusive band, identical to the one observed for poorly annealed samples. To the extent of our knowledge, the regimes reported here have not been discussed in the literature. It remains an interesting open question to provide further understanding of their underlying physics.

It will be interesting to test experimentally these ideas, as in standard experiments the oscillations are relatively fast and the material becomes softer than in a quasi-static deformation. In fact, when a plastic event occurs, the affected region remains softer for a while. With enough time, this transient local softening is forgotten, but not in general. In our work we neglect completely these dynamical effects. Another point to mention is that, in atomistic simulations, the stationary solid phase shows the presence of “reversible” plastic events [8, 9, 13, 14], which are absent in our present model by choice. We are indeed able to further reproduce such feature by replacing the parabolic wells of the disordered potential with multi wells potentials. Nevertheless, this point is out the scope of this work and will be left for future studies. Finally and more importantly, we hope that our predictions will motivate new research directions in the study of low temperature amorphous materials, from realistic large-scale atomistic simulations to experiments.

METHOD - MODEL

We focus on two dimensional systems. Our goal is to provide a description of the physics of amorphous materials under deformation and we use a model based on the evolution of the three strain field components [34, 35]: the isotropic compression $\varepsilon_1(\mathbf{r})$ and the shear components $\varepsilon_2(\mathbf{r})$ and $\varepsilon_3(\mathbf{r})$. The latter are bi-axial deformations (compression along some direction, expansion perpendicularly), the difference between $\varepsilon_2(\mathbf{r})$ and $\varepsilon_3(\mathbf{r})$ is that the compression/expansion axis are the $x - y$ axis for the first, and the lines at 45 degrees for the

second (Recall that given the continuum displacement field, $\mathbf{u}(\mathbf{r}) = (u_1(\mathbf{r}), u_2(\mathbf{r}))$, the elements of strain tensor are given by $\varepsilon_{ij}(\mathbf{r}) = \frac{1}{2}(\partial_i u_j(\mathbf{r}) + \partial_j u_i(\mathbf{r}))$. Then $\varepsilon_1(\mathbf{r}) = (\varepsilon_{11}(\mathbf{r}) + \varepsilon_{22}(\mathbf{r}))/2$, $\varepsilon_2(\mathbf{r}) = (\varepsilon_{11}(\mathbf{r}) - \varepsilon_{22}(\mathbf{r}))/2$ and $\varepsilon_3(\mathbf{r}) = \varepsilon_{12}(\mathbf{r})$). For a perfectly elastic solid, one can write the energy of any deformation in terms of a quadratic elastic functional

$$E_{\text{elast.}} = \int d^2 \mathbf{r} (B\varepsilon_1^2 + \mu\varepsilon_2^2 + \mu\varepsilon_3^2), \quad (4)$$

where B and μ are respectively the bulk and shear modulus. Here we use $B = 1$ and $\mu = 1/2$. This purely elastic functional has a single minimum, which corresponds to the undeformed state. When a deformation is applied, it brings the system out of such a minimum; when released, a restoring stress brings the system back to its undeformed state. If we want to take plasticity into account, irreversible deformations should be allowed; for example, the energy landscape may be characterized by multiple local minima separated by finite barriers. Here, we study the response of the material under simple shear. We account for the plastic events by replacing the harmonic term $\mu\varepsilon_3^2$ in Eq. 4 with a disordered potential $V_{\underline{x}}[\mathbf{r}, \varepsilon_3]$ that displays many minima as ε_3 varies. The other two strain components, ε_1 and ε_2 , are expected to remain small, and the quadratic approximation, to hold. The energy functional then becomes

$$E_{\text{plast.}} = \int d^2 \mathbf{r} (B\varepsilon_1^2 + \mu\varepsilon_2^2 + V_{\underline{x}}[\mathbf{r}, \varepsilon_3]) \quad (5)$$

The subscript of $V_{\underline{x}}$ represents an internal degree of freedom. Thus the disorder potential is not a function of the strain field $\varepsilon_3(\mathbf{r})$ only. The origin of that internal degree of freedom is justified as follows: In amorphous materials, the disorder is not generated by immobile impurities but rather by the random-like configurations of the particles position \underline{x} . Plastic events, called *shear transformations*, are localized in space. When an event occurs in the region \mathbf{r} , the particles inside the region rearrange irreversibly from \underline{x} to \underline{x}' . This rearrangement is mimicked in the model by two features.

- First, $\varepsilon_3(\mathbf{r})$ overcomes a local energetic barrier and reach the basin of a new minimum of the disordered potential.
- Second, the basin of the old minimum also modifies irreversibly as new configuration of particles positions imposes a new disorder potential.

In the spirit of keeping only the essence of the physical process involving local plastic events, we model the disorder of each region \mathbf{r} as a collection of pieces of harmonic potential:

$$V_{\text{parab}}(\varepsilon_3) = \mu[(\varepsilon_3 - \varepsilon_{pl})^2 - \varepsilon_w^2], \quad \text{for } |\varepsilon_3 - \varepsilon_{pl}| < \varepsilon_w. \quad (6)$$

The random parameters ε_{pl} and ε_w vary from region to region: ε_{pl} defines the location of the minimum and ε_w ,

the semi-width of the potential. Once the strain ε_3 overcomes the barriers of the parabolic basin a new semi-width ϵ'_w is drawn from a triangular distribution of mean $1/2$ and standard-deviation $1/20$. The new minimum of the potential is updated as follows:

- When ε_3 overcomes the barrier at $\epsilon_{pl} - \epsilon_w$ then the new minimum is located at $\epsilon_{pl} - (\epsilon_w + \epsilon'_w)$
- When ε_3 overcomes the barrier at $\epsilon_{pl} + \epsilon_w$ then the new minimum is located at $\epsilon_{pl} + (\epsilon_w + \epsilon'_w)$.

It is important to stress that once strain ε_3 overcomes the barriers of the parabolic basin the local basin changes irreversibly, even if the ε_3 moves backward.

The three components of the strain field are not independent but obey the St. Venant constraint [34]. As a consequence, the deformation of the material can be described by the evolution of a single component. In particular assuming, in the framework of an overdamped dynamics, that ε_1 and ε_2 relax much faster than ε_3 , we arrive to

$$\partial_t \varepsilon(\mathbf{r}, t) = \int d^2 \mathbf{r}' G(\mathbf{r} - \mathbf{r}') \varepsilon(\mathbf{r}') + \eta_{\underline{x}}(\mathbf{r}, \varepsilon) + \Sigma_{\text{ext}}. \quad (7)$$

Here, $\varepsilon(\mathbf{r}, t)$ has replaced $\varepsilon_3(\mathbf{r}, t)$ for a lighter notation and the kernel $G(\mathbf{r})$ is the long-range Eshelby's propagator. For simple shear, using the method in [35], the propagator can be written in terms of the polar coordinates $\mathbf{r} = (r, \theta_{\mathbf{r}})$ as

$$G(\mathbf{r}) = \frac{2\sqrt{2}B}{\pi r^2} \frac{3 \cos(4\theta_{\mathbf{r}}) - 1}{(3 - \cos(4\theta_{\mathbf{r}}))^2}. \quad (8)$$

Finally, $\eta_{\underline{x}}$ is originated from the disorder potential as $-\partial_{\varepsilon} V_{\underline{x}}$ and Σ_{ext} is the external applied stress.

For our purposes, it is important to control the macroscopic strain instead of the macroscopic stress. In order to achieve this, one can replace Σ_{ext} with $\kappa(\gamma - \bar{\varepsilon})$ in Eq.7 ($\bar{\varepsilon}$ indicates the macroscopic strain defined as the spatial average of $\varepsilon(\mathbf{r})$). For large values of κ , it is expected that

the macroscopic strain $\bar{\varepsilon}$ is close to γ . The slope of the stress-strain curve is given by $2\kappa\mu/(\kappa + 2\mu)$. Here we use $\kappa = 10$ and $\mu = 1/2$, so we get $10/11 \approx 0.91$ used as the initial slope of the stress-strain curve in the main text.

The energy functional defined in Eq.5 can be equivalently written as

$$E_{\text{plast.}}[\varepsilon(\mathbf{r})] = \int d^2 \mathbf{r} e(\mathbf{r}) \\ \text{with } e(\mathbf{r}) \doteq \frac{1}{2} \varepsilon(\mathbf{r}) \int d\mathbf{r}' G(\mathbf{r} - \mathbf{r}') \varepsilon(\mathbf{r}') \\ + V_{\underline{x}}(\mathbf{r}, \varepsilon(\mathbf{r})). \quad (9)$$

Thus our system can be viewed as an elastic manifold $\varepsilon(\mathbf{r})$ (with long-range interactions among all sites) living in an energy landscape where each site has its independent disordered potential. The stress-free energy used in the main text is then defined as the plastic energy per site: $E_{sf} \doteq E_{\text{plast.}}[\varepsilon^*]/L^2$, with $\left. \frac{\delta E_{\text{plast.}}}{\delta \varepsilon(\mathbf{r})} \right|_{\varepsilon^*} = 0$. The energy profiles of the main text are obtained by averaging the local energy to $e(\mathbf{r})$ along the direction of the shear band. We apply quasi-static deformation γ by numerically solving Eq.7 mapped onto a lattice system.

Special care is taken for the initial condition, since we want to mimic different degrees of annealing in our samples. In our model, a well-annealed sample corresponds to an initial condition where the local strains are confined in deep potential wells, while poorly-annealed samples correspond to a strain manifold confined in shallow potential wells. In practice we start from a liquid configuration of local energy basins obtained after a long uniform shear. Then, to prepare samples of different degree of annealing we change the depths of the parabolic wells, ϵ_w . To obtain deeply annealed samples we also align the centers, ϵ_{pl} , to their mean value. Finally, we let the local strain relax to its stress-free configuration, and that makes our initial condition to start the oscillatory deformation. We performed simulations for systems of sizes $N = 32 \times 32, 64 \times 64, 128 \times 128, 256 \times 256$. The data shown in this work correspond to the two largest systems.

-
- [1] D. Bonn, M. M. Denn, L. Berthier, T. Divoux, and S. Manneville, *Rev. Mod. Phys.* **89**, 035005 (2017-08).
 - [2] A. Nicolas, E. E. Ferrero, K. Martens, and J.-L. Barrat, *Rev. Mod. Phys.* **90**, 045006 (2018-12).
 - [3] M. Ozawa, L. Berthier, G. Biroli, A. Rosso, and G. Tarjus, *Proceedings of the National Academy of Sciences* **115**, 6656 (2018).
 - [4] M. Popović, T. W. J. de Geus, and M. Wyart, *Phys. Rev. E* **98**, 040901 (2018).
 - [5] H. J. Barlow, J. O. Cochran, and S. M. Fielding, *Phys. Rev. Lett.* **125**, 168003 (2020).
 - [6] D. Fiocco, G. Foffi, and S. Sastry, *Phys. Rev. Lett.* **112**, 025702 (2014).
 - [7] D. Fiocco, G. Foffi, and S. Sastry, *Phys. Rev. E* **88**, 020301 (2013).
 - [8] I. Regev, T. Lookman, and C. Reichhardt, *Phys. Rev. E* **88**, 062401 (2013).
 - [9] T. Kawasaki and L. Berthier, *Physical Review E* **94**, 022615 (2016).
 - [10] P. Leishangthem, A. D. S. Parmar, and S. Sastry, *Nature Communications* **8**, 14653 EP (2017).
 - [11] P. Das, A. D. S. Parmar, and S. Sastry, "Annealing glasses by cyclic shear deformation," (2020), arXiv:1805.12476 [cond-mat.soft].
 - [12] D. Hexner, A. J. Liu, and S. R. Nagel, *Proceedings of the National Academy of Sciences* **117**, 31690 (2020).
 - [13] M. Mungan, S. Sastry, K. Dahmen, and I. Regev, *Phys. Rev. Lett.* **123**, 178002 (2019).
 - [14] I. Regev, J. Weber, C. Reichhardt, K. A. Dahmen, and T. Lookman, *Nature Communications* **6**, 8805 EP

- (2015).
- [15] H. Bhaumik, G. Foffi, and S. Sastry, “The role of annealing in determining the yielding behavior of glasses under cyclic shear deformation,” (2019), [arXiv:1911.12957 \[cond-mat.dis-nn\]](https://arxiv.org/abs/1911.12957).
- [16] P. Das, H. Vinutha, and S. Sastry, *Proceedings of the National Academy of Sciences* **117**, 10203 (2020).
- [17] S. Mitra, G. Foffi, A. D. Parmar, P. Leishangthem, and S. Sastry, [arXiv preprint arXiv:2006.15185](https://arxiv.org/abs/2006.15185) (2020).
- [18] M. Ozawa, L. Berthier, G. Biroli, and G. Tarjus, *Phys. Rev. Research* **2**, 023203 (2020).
- [19] M. Singh, M. Ozawa, and L. Berthier, *Phys. Rev. Materials* **4**, 025603 (2020).
- [20] W.-T. Yeh, M. Ozawa, K. Miyazaki, T. Kawasaki, and L. Berthier, *Phys. Rev. Lett.* **124**, 225502 (2020).
- [21] I. Regev and T. Lookman, in *Avalanches in Functional Materials and Geophysics* (Springer, 2017) pp. 227–259.
- [22] I. Regev and T. Lookman, *Journal of Physics: Condensed Matter* **31**, 045101 (2018).
- [23] N. V. Priezjev, *Phys. Rev. E* **93**, 013001 (2016).
- [24] N. V. Priezjev, *Phys. Rev. E* **95**, 023002 (2017).
- [25] J. Lin, E. Lerner, A. Rosso, and M. Wyart, *Proceedings of the National Academy of Sciences* **111**, 14382 (2014).
- [26] I. Fernández Aguirre and E. A. Jagla, *Phys. Rev. E* **98**, 013002 (2018-07).
- [27] E. E. Ferrero and E. A. Jagla, *Phys. Rev. Lett.* **123**, 218002 (2019-11).
- [28] D. S. Fisher, *Phys. Rep.* **301**, 113 (1998).
- [29] E. Agoritsas, V. Lecomte, and T. Giamarchi, *Phys. B: Cond. Matt.* **407**, 1725 (2012).
- [30] E. E. Ferrero, S. Bustingorry, A. B. Kolton, and A. Rosso, *Comptes Rendus Physique* **14**, 641 (2013).
- [31] E. Jagla, *Journal of Statistical Mechanics: Theory and Experiment* **2010**, P12025 (2010).
- [32] D. V. Denisov, M. T. Dang, B. Struth, A. Zaccone, G. H. Wegdam, and P. Schall, *Scientific reports* **5**, 1 (2015).
- [33] S. Sastry, “Models for the yielding behaviour of amorphous solids,” (2020), [arXiv:2012.06726 \[cond-mat.soft\]](https://arxiv.org/abs/2012.06726).
- [34] E. A. Jagla, *Phys. Rev. E* **76**, 046119 (2007).
- [35] X. Cao, A. Nicolas, D. Trimcev, and A. Rosso, *Soft matter* **14**, 3640 (2018).